Powder Technology 241 (2013) 85–97

Contents lists available at SciVerse ScienceDirect

Powder Technology

journal homepage: www.elsevier.com/locate/powtec

Multi-component population balance modeling of continuous granulation processes: A parametric study and comparison with experimental trends

Dana Barrasso [a], Samjit Walia [b], Rohit Ramachandran [a,*]

[a] Department of Chemical and Biochemical Engineering, Rutgers, The State University of New Jersey, Piscataway, NJ 08854, USA
[b] Department of Chemical Engineering, The Cooper Union, New York, NY 10003, USA

ARTICLE INFO

Article history:
Received 16 August 2012
Received in revised form 25 January 2013
Accepted 1 March 2013
Available online 13 March 2013

Keywords:
Continuous granulation
Population balance modeling
Twin-screw
Multi-component
Liquid distribution

ABSTRACT

In the recent few years, continuous processing has been considered as a promising process alternative to batch processing in pharmaceutical manufacturing. Via a novel population balance model framework, a multi-dimensional multi-component model for a continuous granulation process was developed, describing time evolutions of distributions with respect to granule size, liquid distribution and granule composition. A parametric study was performed to analyze the effects of various process and design parameters, including granulator size and configuration, liquid spray rate and particle velocity, on evolutions and distributions of key granule properties. Simulation results capture experimentally observed sensitivities and trends thus demonstrating the use of a model-based framework for granulation process design, control and optimization to enable QbD in drug product development.

1. Introduction

Granulation is a particle design process in which fine powder particles agglomerate to form larger granules with improved properties, such as flowability, reduced dust formation, and composition uniformity. In wet granulation processes, aggregation is facilitated with the addition of a liquid binder. Wet granulation is governed by three rate processes; wetting and nucleation, consolidation and aggregation, and attrition and breakage [1,2].

Granulation processes are utilized in various process industries, such as food, pharmaceuticals, and fertilizers [1]. Because a narrow size distribution is often desired, industrial granulation processes are typically inefficient, with large recycle ratios of up to 6:1 [3]. As a result, design, scale up, and control of granulation processes are usually based on heuristic experimentation. Particularly in the pharmaceutical industry, granule composition, in addition to other granule properties such as liquid content and porosity, must be controlled to ensure product uniformity that meets strict regulatory guidelines [4].

Pharmaceutical manufacturing processes are almost exclusively operated in batch configurations. However, continuous processing has gained recent attention due to its numerous potential advantages over batch processes [5–7,4,8]. For instance Schaber et al. [8] predicted substantial economic benefits of continuous manufacturing. However, Vervaet and Remon [4] caution against the common misconceptions surrounding continuous processing in the pharmaceutical industry, such as the idea that continuous processes on their own cannot always consistently meet the quality requirements of the highly regulated industry. Instead, they argue that real-time monitoring using in-line process analytical techniques (PAT) would result in better process control, higher efficiencies, and less destruction of product due to failed specifications.

In order to successfully transition to continuous processing, significant process understanding must be developed. A model-based approach to design and control of continuous powder processes has been proposed to tackle this challenge [9,3]. This approach can be used to define a design space, and if the process variables are kept within the design space, the product will be of acceptable quality, a concept known as Quality by Design (QbD). For instance, Glaser et al. [10] and Ramachandran et al. [11,12] have demonstrated model-based control methods for continuous granulation using population balance modeling. Additionally, Boukouvala et al. [13–15] have developed data-driven models for continuous powder processes.

1.1. Continuous granulation

A typical continuous horizontal granulator is divided into three zones. The first zone is the premixing zone, where dry powder particles are fed and mixed to achieve blend homogeneity. The particles then move into the spray zone, where liquid binder is sprayed onto the particles, and they begin to nucleate and aggregate to form larger granules. After the spray zone, the particles pass through a wet-massing zone, where they continue to aggregate and consolidate due to residual liquid and collisions, forming larger and denser granules. Other mechanisms

* Corresponding author. Fax: +1 732 445 2581.
E-mail address: rohit.r@rutgers.edu (R. Ramachandran).

0032-5910/$ – see front matter © 2013 Elsevier B.V. All rights reserved.
http://dx.doi.org/10.1016/j.powtec.2013.03.001

such as breakage and layering may also occur concurrently in the spray and wet massing zone.

Continuous wet granulation processes can be categorized into four types: fluidized bed, twin screw, high shear, and drum granulation. Horizontal fluidized bed granulators are often used in industries with high product volumes, such as the food industry [4]. These machines can include dryers, removing the need for a separate drying step.

In twin screw granulation, two screws transport the particles through an extruder, mixing them in the process. This technique has been widely studied for pharmaceutical applications [16,4,17], particularly because it is suitable for various capacities [4]. However, a separate drying step is necessary to produce dry granules. Additionally, the screw configuration can become an important design parameter.

A high shear mixer can also be used for granulation with the addition of sprayers. This process is similar to twin screw granulation, using an impeller to transport the particles instead of screws. High shear granulation also produces wet granules, and it often is operated at a higher capacity than twin screw granulation [4].

Finally, a continuous drum granulator consists of a rotating cylinder, operating at a lower shear rate than high shear granulation. The cylinder is slightly inclined to transport the material. Continuous drum granulation is commonly used in the fertilizer industry [18].

1.2. Population balance models

The population balance model (PBM) framework tracks the number of particles with a given set of properties (e.g. size) as they are subject to rate processes, such as aggregation, nucleation, and breakage. PBMs are often used to model powder processes, such as crystallization, mixing, milling, and granulation. The general population balance equation is given in Eq. (1) [19].

$$\frac{\partial F(\mathbf{x},t)}{\partial t}+\sum\frac{\partial}{\partial \mathbf{x}}\left[F(\mathbf{x},t)\frac{d\mathbf{x}}{dt}(\mathbf{x},t)\right]=\Re_{\text{formation}}(\mathbf{x},t)-\Re_{\text{depletion}}(\mathbf{x},t). \quad (1)$$

Here, F is the number of particles or particle density with the set of properties described by the vector $\mathbf{x}$. This vector $\mathbf{x}$ is often composed of the internal coordinates of solid, liquid, and gas volumes. The first term of this equation describes the rate of change of particle density, and the second term accounts for changes along one internal coordinate, such as liquid addition, consolidation, or layering. The formation and depletion rates, $\Re_{\text{formation}}$ and $\Re_{\text{depletion}}$, account for net changes due to aggregation, nucleation, and breakage.

A three-dimensional (3-D) PBM has also been employed to model granulation processes [20–25]. As shown in Eq. (2), this model accounts for simultaneous distributions of solid, liquid, and gas volumes.

$$\frac{\partial}{\partial t}F(s,l,g,t)+\frac{\partial}{\partial s}\left[F(s,l,g,t)\frac{ds}{dt}\right]+\frac{\partial}{\partial l}\left[F(s,l,g,t)\frac{dl}{dt}\right]+\frac{\partial}{\partial g}\left[F(s,l,g,t)\frac{dg}{dt}\right]=\Re_{\text{nuc}}+\Re_{\text{agg}}+\Re_{\text{break}}. \quad (2)$$

This model includes terms for solid layering $\left(\frac{ds}{dt}\right)$, liquid addition $\left(\frac{dl}{dt}\right)$, gas consolidation $\left(\frac{dg}{dt}\right)$, net rates of nucleation $(\Re_{\text{nuc}})$, aggregation $(\Re_{\text{agg}})$, and breakage $(\Re_{\text{break}})$. To fully model multi-component granulation, a fourth dimension must be added for the second solid component. However, higher-order PBMs are computationally expensive, and a four-dimensional PBM can take days or weeks to solve [26]. Higher-order PBMs can be reduced by assuming that one or more properties that are less significant are lumped within the other distributions [26].

The PBM can be extended to include spatial coordinates to model non-uniform batch processes and continuous processes [19]. As shown in Eq. (3), a vector of external coordinates ($\mathbf{z}$) is added, accounting for spatial distributions in particle frequencies and properties.

$$\frac{\partial F(\mathbf{x},\mathbf{z},t)}{\partial t}+\frac{\partial}{\partial \mathbf{x}}\left[F(\mathbf{x},\mathbf{z},t)\frac{d\mathbf{x}}{dt}(\mathbf{x},\mathbf{z},t)\right]+\frac{\partial}{\partial \mathbf{z}}\left[F(\mathbf{x},\mathbf{z},t)\frac{d\mathbf{z}}{dt}(\mathbf{x},\mathbf{z},t)\right]=\Re_{\text{formation}}(\mathbf{x},\mathbf{z},t)-\Re_{\text{depletion}}(\mathbf{x},\mathbf{z},t)+\dot{F}_{\text{in}}(\mathbf{x},\mathbf{z},t)-\dot{F}_{\text{out}}(\mathbf{x},\mathbf{z},t). \quad (3)$$

The term $\frac{dg}{dt}$ represents the particle velocity, and $\dot{F}_{\text{in}}$ and $\dot{F}_{\text{out}}$ are the inflow and outflow rates.

1.3. Previous applications of PBMs

One-dimensional (1-D) PBMs are most commonly used for batch and continuous modeling because they are easy to solve and computationally inexpensive [27,28,26]. These models account for distributions with respect to one particle property, usually size. For granulation processes, this assumption has been found to be inefficient since other particle properties such as liquid content and porosity can significantly affect aggregation rates [27,29,26]. Additionally, 1-D PBMs cannot represent distributions of key product quality attributes such as granule composition.

Most previous multi-dimensional PBM studies of wet granulation have involved batch processes [23,21,30]. These PBMs often focus on distributions in size, porosity, and liquid content, without simulating multiple solid components. However, Matsoukas and Marshall [31] have developed a solid composition-dependent aggregation rate kernel. Marshall et al. [32] presented a multi-component PBM for batch granulation to analyze the effects of binder content distribution, and Lee et al. [33] have investigated segregation of solid components in batch granulation. In a previous study, Barrasso and Ramachandran [26] presented a four-dimensional model for batch granulation, considering size, porosity, liquid content, and composition.

Fewer models of continuous granulation have been developed. Heinrich et al. [34,35] presented a dynamic 1-D PBM of continuous fluidized bed granulation, which did not include spatial coordinates. Further, Vreman et al. developed dynamic and steady state 1-D models for fluid bed granulation. Wang and Cameron [3] reviewed the progress in modeling continuous drum granulation for control applications. Although these 1-D models are useful for design and optimization, they cannot capture inhomogeneities and spatial effects. For use in a control study, Ramachandran and Chaudhury [11] have developed a 3-D PBM of continuous drum granulation that models spatial coordinates in three compartments. PBMs have also been used to model other continuous powder processes, such as crystallization and mixing [36,37]. No studies were found that use a PBM to simulate a twin-screw granulation process.

In this study, a 3-D continuous PBM for multi-component twin-screw granulation processes will be presented, accounting for distributions in size, liquid content, and solid composition that vary throughout the granulator.

1.4. Objectives

The purpose of this study is to propose a multi-dimensional model for continuous granulation processes. In particular, the following objectives will be addressed:

- Develop a dynamic 3-D PBM for multi-component, continuous granulation with two spatial dimensions, accounting for the rate processes of aggregation, breakage, liquid addition, and consolidation.
- Demonstrate this model's ability to capture experimental trends and observations based on using data from a twin-screw granulator.
- Perform a parametric study to analyze the effects of various input parameters on steady-state product distributions and start-up dynamics.

2. Model development

In this study, a 3-D PBM was developed to account for simultaneous distributions in size, composition, and liquid binder content, as given in Eq. (4). For the purposes of this study, nucleation and layering effects were neglected. Although nucleation occurs during granulation, aggregation is the primary mechanism of particle growth [38]. However, it can be easily incorporated based on previous work by the second author [21]. Layering was neglected due to previous experimental work ascertaining the layering is minimal in viscous regimes that result in aggregation being the dominant mechanism [22].

$$\frac{\partial}{\partial t}F(s_1,s_2,l,t)+\frac{\partial}{\partial l}\left[F(s_1,s_2,l,t)\frac{\mathrm{d}l}{\mathrm{d}t}\right]=\Re_{\mathrm{agg}}+\Re_{\mathrm{break}}. \tag{4}$$

Here, s_1 and s_2 represent the volumes of excipient and API in each granule, respectively. This model does not include a distributed gas volume. Instead, gas is represented as a lumped parameter under the assumption that all granules of the same size, composition, and liquid binder content have the same averaged porosity. In a previous study, this technique was found to reduce the computational expense significantly with minimal effect on accuracy [26]. The volume of gas in each particle is represented as a function of the API, excipient, and liquid binder volumes and is determined from Eq. (5).

$$\frac{\partial}{\partial t}[G(s_1,s_2,l,t)]+\frac{\partial}{\partial l}\left[G(s_1,s_2,l,t)\frac{\mathrm{d}l}{\mathrm{d}t}\right]=F(s_1,s_2,l,t)\frac{\mathrm{d}g}{\mathrm{d}t}+\Re_{\mathrm{agg,gas}}+\Re_{\mathrm{break,gas}}. \tag{5}$$

In this equation, G represents the total volume of gas in a bin, and g is the average volume of gas per particle in that bin. $\Re_{\mathrm{agg,gas}}$ and $\Re_{\mathrm{break,gas}}$ correspond to the amount of gas transferred due to aggregation and breakage.

The internal coordinates of API, excipient, liquid, and gas volumes are related to key granule properties, such as size, porosity, liquid binder content, and solid composition. A homogeneous product is desired, with narrow distributions in these attributes. The relationships between the internal coordinates and granule properties are given in Table 1.

2.1. Spatial coordinates and particle flow

By adding external coordinates, the 3-D model was adapted to suit continuous granulation processes. The granulator was represented by two spatial dimensions, as done in previous mixing and powder flow studies [39,37]. The resulting continuous population balance equations are given in Eqs. (6) and (7).

$$\frac{\partial}{\partial t}F(s_1,s_2,l,x,y,t)+\frac{\partial}{\partial l}\left[F(s_1,s_2,l,x,y,t)\frac{\mathrm{d}l}{\mathrm{d}t}\right]+\frac{\partial}{\partial x}\left[F(s_1,s_2,l,x,y,t)\frac{\mathrm{d}x}{\mathrm{d}t}\right]+\frac{\partial}{\partial y}\left[F(s_1,s_2,l,x,y,t)\frac{\mathrm{d}y}{\mathrm{d}t}\right]=\dot{F}_{\mathrm{in}}(s_1,s_2,l,x,y,t)-\dot{F}_{\mathrm{out}}(s_1,s_2,l,x,y,t)+\Re_{\mathrm{agg}}+\Re_{\mathrm{break}}. \tag{6}$$

Table 1
Granule properties and dependent rate processes.

Granule property	Definition	Dependent rate processes
Size (volume)	$V=s_1+s_2+l+g$	Aggregation, breakage, consolidation
Size (diameter)	$d=\left[\frac{6\times(s_1+s_2+l+g)}{\pi}\right]^{(1/3)}$	Aggregation, breakage, consolidation
Solid composition	$x=\frac{s_1}{s_1+s_2}$	Aggregation
Liquid binder content	$l_s=\frac{l}{s_1+s_2+l+g}$	Aggregation
Porosity	$\epsilon=\frac{l+g}{s_1+s_2+l+g}$	Consolidation

$$\frac{\partial}{\partial t}G(s_1,s_2,l,x,y,t)+\frac{\partial}{\partial l}\left[G(s_1,s_2,l,x,y,t)\frac{\mathrm{d}l}{\mathrm{d}t}\right]+\frac{\partial}{\partial x}\left[G(s_1,s_2,l,x,y,t)\frac{\mathrm{d}x}{\mathrm{d}t}\right]+\frac{\partial}{\partial y}\left[G(s_1,s_2,l,x,y,t)\frac{\mathrm{d}y}{\mathrm{d}t}\right]=F(s_1,s_2,l,x,y,t)\frac{\mathrm{d}g}{\mathrm{d}t}+g_{\mathrm{in}}\dot{F}_{\mathrm{in}}(s_1,s_2,l,x,y,t)-g_{\mathrm{out}}\dot{F}_{\mathrm{out}}(s_1,s_2,l,x,y,t)+\Re_{\mathrm{gas,agg}}+\Re_{\mathrm{gas,break}}. \tag{7}$$

The axial and radial dimensions refer to the location of the particles within the granulator and are represented by x and y, respectively. These bins span the length of the granulator, covering all three zones. The terms $\frac{dx}{dt}$ and $\frac{dy}{dt}$ represent the axial and radial particle velocities, which can vary over time and position. Additionally, the inflow and outflow of particles in the feed and product are given by $\dot{F}_{\mathrm{in}}$ and $\dot{F}_{\mathrm{out}}$, respectively. The inflow term is based on an overall mass flow rate, $\dot{m}_{\mathrm{in}}$, and feed particle distribution p_{in}, as well as the powder density ρ, as shown in Eq. (8).

$$\dot{F}_{\mathrm{in}}(s_1,s_2,l)=\frac{\dot{m}_{\mathrm{in}}}{\rho}\frac{p_{\mathrm{in}}(s_1,s_2,l)}{V(s_1,s_2,l)}. \tag{8}$$

The inlet flow rate, distribution, and density are given in Table 2. The outlet flow rate is based on the particle velocity and distribution in the last axial bin. All simulations are performed from process startup, so the initial number of particles within the granulator is zero.

The geometry of the granulator was defined to be consistent with the EuroLab 16 mm twin screw granulator (L:D of 40:1) located at the Purdue University National Science Foundation (NSF) Engineering Research Center for Structured Organic Particulates (ERC-SOPs) facility. A diagram of this geometry is presented in Fig. 1. This approach can also be used for high shear or fluidized bed granulation, and differences between the granulator types appear in input parameters such as particle velocity profiles, shear rates, and granulator geometry.

To determine the particle velocities, the PBM can be coupled with discrete element modeling (DEM) [37]. For this study, an average axial velocity was assumed based on experimentally observed residence times in the granulator [17]. A normal distribution of random numbers was used to vary this velocity at each time point and

Table 2
Process parameters and initial conditions used in simulations for the baseline case.

Parameter name	Symbol	Baseline value
Mass flow rate of feed particles	$\dot{m}_{\mathrm{in}}$	4 kg/h
Mass fraction of excipient particles in feed	$\dot{p}_{\mathrm{in}}(2,1,1)$	0.75
Mass fraction of API particles in feed	$\dot{p}_{\mathrm{in}}(1,2,1)$	0.25
Density of feed particles	ρ	1525 kg/m^3
Volume of gas per particle in feed	g_{in}	2.67×10^{-13} m^3
Mean axial velocity (standard deviation)	v_x	0.03 m/s(0.01 m/s)
Mean radial velocity (standard deviation)	v_y	0 m/s(0.003 m/s)
Granulator length	x_f	0.32 m
Granulator diameter	y_f	0.016 m
Axial bounds on spray zone	x_1, x_2	0.08 m, 0.16 m
Radial bounds on spray zone (homogeneous distribution)	y_1, y_2	0 m, 0.016 m
Radial bounds on spray zone (heterogeneous distribution)	y_1, y_2	0.012 m, 0.016 m
Time at which sprayer turns on	t_{spray}	5 s
Liquid to solid ratio	L/S	0.15
Aggregation constants	$\beta_0, \alpha, \delta, a_{ab}$	300, 1, 1, 0
Breakage constants	P_1, P_2	1, 1
Shear rate	G_{shear}	20 s^{-1}
Consolidation constant	c	0.001 s^{-1}
Minimum porosity	ϵ_{min}	0.1
Volume of smallest excipient bin	$s_{1,1}$	2×10^{-13} m^3
Volume of smallest API bin	$s_{2,1}$	2×10^{-13} m^3
Volume of smallest liquid binder bin	l_1	1×10^{-13} m^3
Number of bins	$(i,j,k)_{\mathrm{max}}$	(8,8,8)
Time step	Δt	0.01 s

position. The average values and standard deviations are given in Table 2. Future work is needed to better understand the particle velocity profiles inside the granulator either via particle velocimetry or DEM studies.

2.2. Rate processes

2.2.1. Liquid addition

In continuous wet granulation, liquid binder is sprayed on dry particles within the spray zone, as shown in Fig. 1. Liquid is added at a constant rate of $\dot{V}_{spray}$, and as the particles pass through the spray zone, their liquid content increases, resulting in higher aggregation rates. The expression for the liquid addition term is given in Eq. (9).

$$\frac{dl}{dt} = \frac{\dot{V}_{spray}}{\int_{y_1}^{y_2}\int_{x_1}^{x_2}\int_0^{\infty}\int_0^{\infty}\int_0^{\infty} F(s_1,s_2,l,x,y,t)\ ds_1\ ds_2\ dl\ dx\ dy}. \tag{9}$$

$\frac{dl}{dt}$ is the volumetric rate of liquid addition per particle, which was assumed to be equal for all particles within the spray zone, and $F(s_1,s_2,l,x,y,t)$ is the full distribution of particles with respect to API, excipient, and liquid volume as well as the spatial position. The liquid spray rate is described by a liquid to solid ratio, where $L/S = \rho\dot{V}_{spray}/\dot{m}_{in}$. In these simulations, the sprayer is turned on shortly after the process begins so that some particles reach the spray zone before liquid is added. Aggregation and breakage rates of wet granules were considered negligible prior to the start of liquid addition, due to the absence of liquid binder.

The spatial limits of integration (x_1,x_2,y_1, and y_2) describe the axial and radial boundaries of the spray zone. While the axial boundaries are defined by the position of the sprayer, the radial boundaries depend on how well the liquid is distributed throughout the powder. For continuous twin screw granulation, Dhenge et al. [40] found that low viscosity liquids are distributed more uniformly than high viscosity liquids. El Hagrasy et al. [17] demonstrated the need to improve liquid distribution in twin screw granulation and showed that poor liquid binder distribution resulted in wide granule size distributions. To investigate this issue, two cases are modeled. The first case assumes that the liquid is evenly distributed in the radial direction, and the interval from y_1 to y_2 encompasses all radial bins. The second case simulates poor liquid binder distribution, such that only one radial bin receives the liquid. The liquid spreads to the other bins through radial movement of particles.

The values used for the spray rate, the time at which spray is added (t_{spray}), and the spray zone for both cases are included in Table 2. Since the liquid addition rate depends on the number of particles in each bin, it is recalculated at each time step.

2.2.2. Aggregation

In the aggregation process, two particles collide and merge to form one larger particle. The rate of aggregation depends on the number of particles and their properties. As shown in Eq. (10), the net aggregation rate can be broken into formation and depletion rates.

$$\Re_{agg}(s_1,s_2,l,t) = \Re_{agg}^{form}(s_1,s_2,l,t) - \Re_{agg}^{dep}(s_1,s_2,l,t). \tag{10}$$

These rates are determined using the particle distribution function F and a semi-empirical aggregation kernel β and are defined in Eqs. (11) and (12).

$$\Re_{agg}^{form}(s_1,s_2,l,t) = \frac{1}{2}\int_0^{s_1}\int_0^{s_2}\int_0^{l} \beta(s_1-s_1',s_2-s_2',l-l',s_1',s_2',l') \times F(s_1-s_1',s_2-s_2',l-l',t)F(s_1',s_2',l',t)\ dl'\ ds_2'\ ds_1' \tag{11}$$

$$\Re_{agg}^{dep}(s_1,s_2,l,t) = F(s_1,s_2,l,t) \times \int_0^{\infty}\int_0^{\infty}\int_0^{\infty} \beta(s_1,s_2,l,s_1',s_2',l')F(s_1',s_2',l',t)\ dl\ ds_2\ ds_1. \tag{12}$$

The aggregation kernel takes particle properties into account. For example, a high liquid binder content is known to increase the aggregation rate. A variety of aggregation kernels are available in the literature [2]. Shown in Eq. (13), the aggregation kernel presented by Madec et al. [41] was selected because of its liquid content and size dependencies.

$$\beta(s_1,s_2,l,s_1',s_2',l') = \beta_0(V+V')\left((l_s+l_s')^{\alpha}\left(100-\frac{l_s+l_s'}{2}\right)^{\delta}\right)^{\alpha}. \tag{13}$$

The two colliding particles are described by the internal coordinates (s_1,s_2,l) and (s_1',s_2',l'), and V and l_s represent their respective volumes and liquid contents. Selected values for the three adjustable parameters, β_0, α, and δ, are given in Table 2.

This kernel does not account for interactions between the two solid components, which can be attractive or repulsive. Because the product composition distribution is a key quality attribute of this process, a composition dependent aggregation kernel is desired to simulate these interactions. To modify a size-dependent aggregation kernel, a composition-dependent multiplicative factor was proposed by Matsoukas et al. [42], as given by Eq. (14).

$$\psi(s_1,s_2,s_1',s_2') = \exp(-a_{ab}(x+x'-2xx')). \tag{14}$$

The adjustable interaction parameter a_{ab} describes the attraction or repulsion of the two components. If a_{ab} is greater than zero, the solid components are repulsive, and if a_{ab} is less than zero, they are attractive [42]. This factor was used with the size- and liquid content-dependent aggregation kernel (Eq. (13)) to introduce composition dependence, resulting in the overall aggregation kernel shown in Eq. (15).

$$\beta(s_1,s_2,l,s_1',s_2',l') = \beta_0(V+V')\left((l_s+l_s')^{\alpha}\left(100-\frac{l_s+l_s'}{2}\right)^{\delta}\right)^{\alpha} \times \exp(-a_{ab}(x+x'-2xx')). \tag{15}$$

2.2.3. Breakage

When particles are subject to impact or attrition, they can break into two or more fragments. Like the aggregation rate, the breakage rate can be broken into formation and depletion terms, as shown in

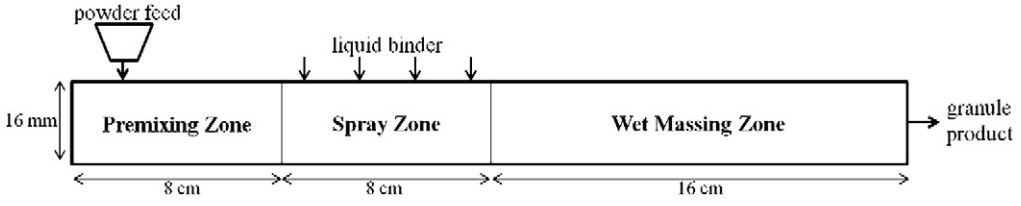

Fig. 1. Continuous granulator with three zones.

Eq. (16). The formation rate of smaller fragments, $\Re_{break}^{dep}$, and the depletion rate of larger granules, $\Re_{break}^{form}$, are presented in Eqs. (17)–(18).

$$\Re_{break}(s_1,s_2,l,t) = \Re_{break}^{form}(s_1,s_2,l,t) - \Re_{break}^{dep}(s_1,s_2,l,t) \tag{16}$$

$$\Re_{break}^{form}(s_1,s_2,l,t) = \int_0^{\infty}\int_0^{\infty}\int_0^{\infty} K_{break}(s_1',s_2',l')b(s_1',s_2',l',s_1,s_2,l)F(s_1',s_2',l',t)\ dl'\ ds_2'\ ds_1' \tag{17}$$

$$\Re_{break}^{dep}(s_1,s_2,l,t) = K_{break}(s_1,s_2,l)F(s_1,s_2,l,t). \tag{18}$$

The breakage kernel, K_{break}, describes the likelihood of breakage for a parent particle, and the probability distribution function, b, determines the size of the resulting fragments.

A semi-empirical breakage kernel was used, as shown in Eq. (19) [43].

$$K_{break}(s_1,s_2,l) = \frac{P_1 G_{shear} d^{P_2}}{2}. \tag{19}$$

This kernel is dependent on the diameter of the parent particle, d, as a larger particle is more likely to break than a smaller one. It is also dependent on the shear rate, G_{shear}. The shear rate can vary throughout a continuous granulator, particularly in a twin-screw granulator that includes various screw elements. For this study, a constant and uniform shear rate was used, given in Table 2. Further research is needed to model the shear rate distribution more accurately. P_1 and P_2 are adjustable constants whose values are also provided in Table 2.

In this study, it was assumed that all breakage events result in two fragments. The probability distribution is given by Eq. (20).

$$b(s_1',s_2',l',s_1,s_2,l) = \frac{1}{(i-1)(j-1)(k-1)} \text{for } (s_1,s_2,l) < (s_1',s_2',l'). \tag{20}$$

The indices i, j, and k represent the parent particle bin numbers of each solid component and the liquid binder, respectively. This distribution assumes the fragment particles have an equal likelihood of forming in each bin smaller than the parent particle.

2.2.4. Consolidation

As the particles are compacted, consolidation occurs and the volume of gas contained within the particles decreases. The rate of consolidation is described by Eq. (21), which is consistent with an exponential decrease of porosity [29].

$$\frac{dg}{dt} = -c\frac{(s_1+s_2+l+g)(1-\epsilon_{min})}{s_1+s_2}\left[l - \frac{\epsilon_{min}(s_1+s_2)}{1-\epsilon_{min}} + g\right]. \tag{21}$$

The minimum granule porosity, ϵ_{min}, and the consolidation rate constant, c, are given in Table 2 based on the work of Immanuel and Doyle III [20].

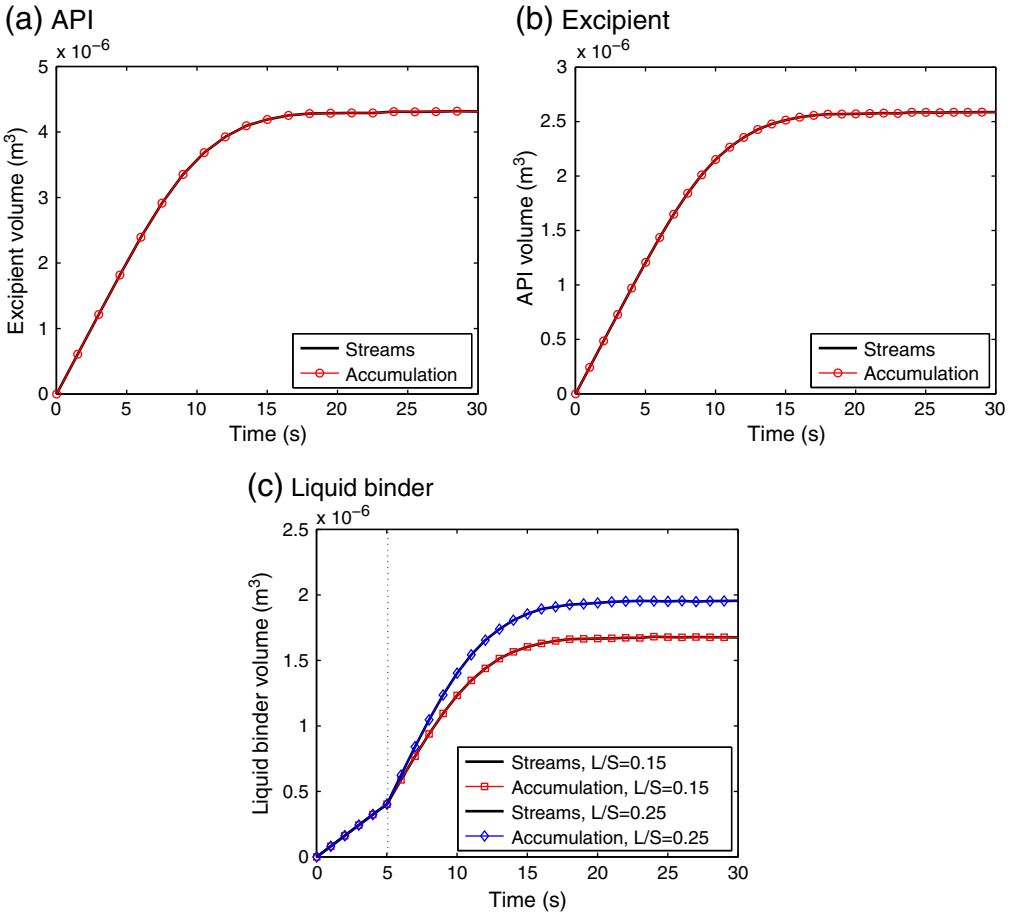

Fig. 2. Total volume of each component within the granulator over time, calculated from the inlet and outlet streams and from the distribution of particles accumulated within the granulator. These plots are based on the baseline case with heterogeneous liquid distribution and a simulation with a larger L/S ratio. The vertical dotted line indicates the time at which spraying begins.

2.3. Discretization and numerical techniques

To solve the population balance equation numerically, a finite difference method was used. The spatial and internal dimensions were discretized, creating a system of ordinary differential equations. The granulator was divided into discrete spatial bins, using eight evenly-spaced axial bins, covering the three zones, and four evenly-spaced radial bins. A non-linear grid was used for the internal coordinates in order to accommodate particles of large sizes with a minimal number of bins. These grids are described by Eqs. (22)–(24).

$$s_{1,i} = s_{1,1} \times 3^{i-1} \tag{22}$$

$$s_{2,j} = s_{2,1} \times 3^{j-1} \tag{23}$$

$$l_k = l_1 \times 3^{k-1}. \tag{24}$$

In these equations, i, j, and k represent the indices of the first solid component, second solid component, and liquid bins, respectively, and $s_{1,i}$, $s_{2,j}$, and l_k represent the corresponding volumes of each component per particle. The volume of the smallest bin, $(s_{1,1}, s_{2,1}, l_1)$, and the number of bins can be found in Table 2. The inlet population density was distributed over two internal bins, (1, 2, 1) and (2, 1, 1), to simulate particles of two different solid compositions, such as an API and an excipient. Because the volumes of each component in the first bin are nonzero, the feed particles are not represented as pure components. The lumped parameter, the gas volume, does not require discretization. The inlet gas volume per particle is also provided in Table 2.

Because a nonlinear grid was used, aggregating or breaking particles can have volumes that lie between bins. The cell average method was used to allocate these particles into the surrounding bins, as demonstrated by Kumar et al. [44] for the 1-D case and by Chaudhury et al. [45] for multi-dimensional cases. This method conserves the volume of all components.

The system of equations was integrated numerically using first-order Euler integration. Since an explicit integration technique was used, the Courant–Friedrichs–Lewis (CFL) condition must be satisfied for numerical stability [24]. The CFL condition states that the time step must have a maximum value above which the solution will be inaccurate. In this case, the time step must be less than the time required for particles to travel to adjacent grid points. The selected time step is given in Table 2.

These computations were performed using MATLAB on an Intel Core i7-2600 CPU processor (3.4 GHz) with 16 GB of RAM.

3. Results and discussion

3.1. Validation of numerical methods

Several techniques were used to demonstrate the effectiveness of the numerical methods. First, the simulations demonstrated conservation of API, excipient, and liquid binder, as shown in Fig. 2 for the baseline case. The stream curves are the net volume of material transferred from the inlet and outlet streams to the granulator, and the accumulation curves represent the total volume of the material within the granulator, based on the particle distributions. The streams and accumulation curves are consistent, demonstrating that the volumes of these components are conserved.

Additionally, the ratios of birth to depletion for aggregation and breakage must be consistent with the assumptions in the problem, which stated that two particles aggregate to form one larger particle during aggregation, and each fracturing particle forms two particles. As shown in Fig. 3, the ratios of birth to depletion for aggregation and breakage are 0.5 and 2, respectively.

First-order explicit Euler integration was used to solve this system of ordinary differential equations. This integration technique requires only one function evaluation at each time step, whereas multistep, adaptive, and implicit methods require multiple function evaluations or iterations at each time step. An explicit, second-order Runge–Kutte method (RK2) was used to solve the baseline case for comparison with Euler integration. At the selected time step size, Euler integration produced nearly the same results as RK2, demonstrating sufficient accuracy. Fig. 4 shows the number of particles in three specific bins over time using Euler and RK2 integration. Euler integration solved the problem 50.03% more quickly than RK2 integration. Therefore, the Euler integration method was utilized in this study.

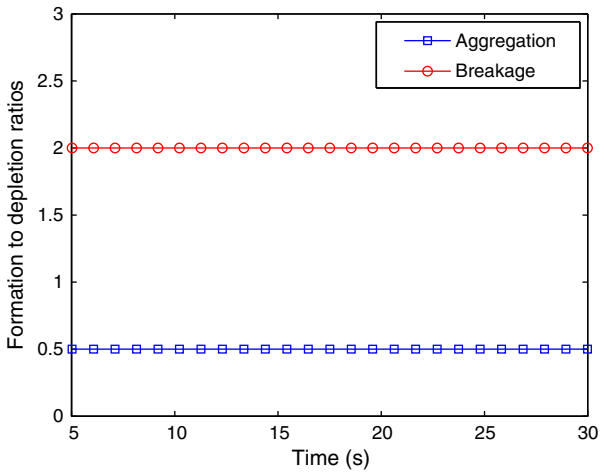

Fig. 3. Ratios of formation to depletion for aggregation and breakage for the baseline case with heterogeneous liquid distribution.

Finally, the grid independence of the model was investigated. Keeping the upper and lower bounds constant, the grid size was varied by changing the base value in Eqs. (22)–(24). Plots of the steady-state particle size distribution with various grid sizes are shown in Fig. 5. A marginal difference was observed, with a difference of approximately 1.2% between the steady-state diameters predicted using 8 and 9 bins. More accurate results are expected when using a finer grid width and smaller time step. However, this can drastically increase computation time.

3.2. Parametric study

A parametric study was performed to evaluate the effects of material, process, and design parameters, including the liquid binder distribution,

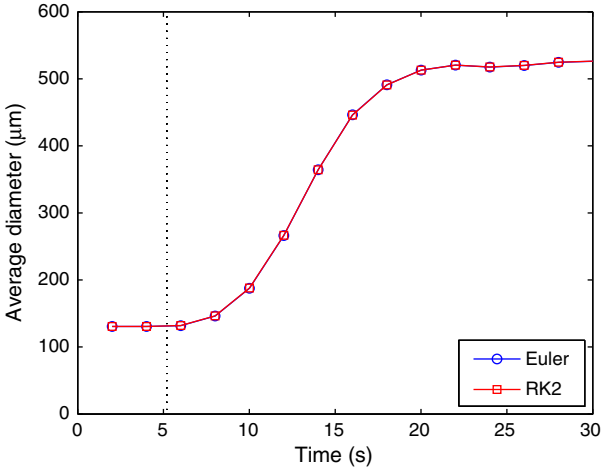

Fig. 4. Average diameter at the outlet vs. time using different integration techniques. The vertical dotted line indicates the time at which spraying begins.

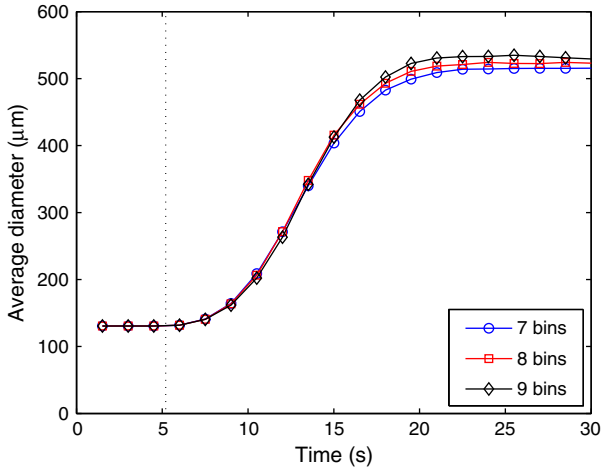

Fig. 5. Average diameter at the outlet vs. time for the baseline case with poor liquid distribution, with varying grid sizes. The vertical dotted line indicates the time at which spraying begins.

liquid to solids ratio, spray zone position and granulator lengths, particle velocities, and API–excipient interactions. In all simulations, the average product particle size increased over time before reaching a steady state. The start-up behavior and steady-state particle size distributions were analyzed, in addition to two-dimensional distributions, such as size and composition. The simulations also showed the granule properties at each position within the granulator. Finally, a pulse change in the powder feed was simulated to analyze the residence time distribution (RTD) for each simulation.

3.2.1. Liquid binder distribution

Two cases for the liquid binder distribution were simulated. In the homogeneous case, the binder was sprayed uniformly on all particles within the spray zone. For the heterogeneous case, liquid binder only reached particles in the highest radial bin, or the top 25% of the granulator. The liquid binder was transferred to other locations and particles through radial movement and aggregation. The same total liquid volume and spray rate were used in each case.

Fig. 6 shows the average product diameter over time for each case. At steady state, the homogeneous case produced slightly larger granules than the heterogeneous case, with average diameters of 548 μm and 523 μm, respectively. Steady-state particle size distributions are given in Fig. 6. The heterogeneous case shows a larger frequency of small particles than the homogeneous case. These results are as expected and can be explained by the aggregation rates. If the liquid is not distributed evenly, some particles remain dry and are less likely to aggregate, represented in the model by the liquid-dependent aggregation kernel. The liquid content particle distributions support this explanation, as shown in Fig. 6.

In Fig. 7, contour plots of size and liquid content versus position within the granulator show that the homogeneous case resembles a plug flow process, while the heterogeneous case has strong variations in both size and liquid content with radial position. In the heterogeneous case, the particles located near the sprayer collect most of the liquid and grow faster than particles located far from the sprayer. Further, the physical separation between the wet and dry particles contributes to the size difference. For the heterogeneous case, the dry particles are near other dry particles, resulting in very low aggregation rates and slow growth. When the liquid distribution is homogeneous, a dry particle can aggregate with a nearby wet particle, and this interaction has a higher aggregation rate than the interaction between two dry particles.

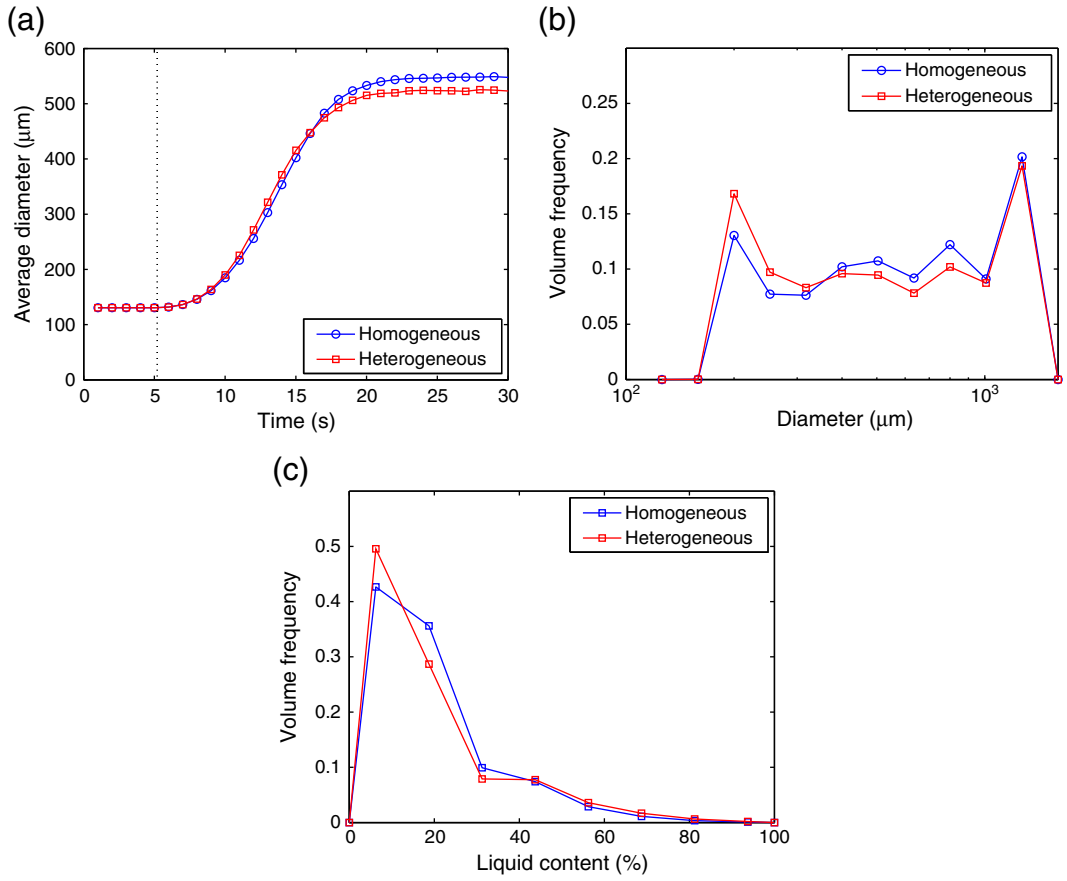

Fig. 6. (a) Average diameter at the outlet vs. time, (b) steady-state particle size distributions at the outlet and (c) steady-state liquid content distribution at the end of the spray zone for the baseline case with both liquid distribution models. The vertical dotted line indicates the time at which spraying begins.

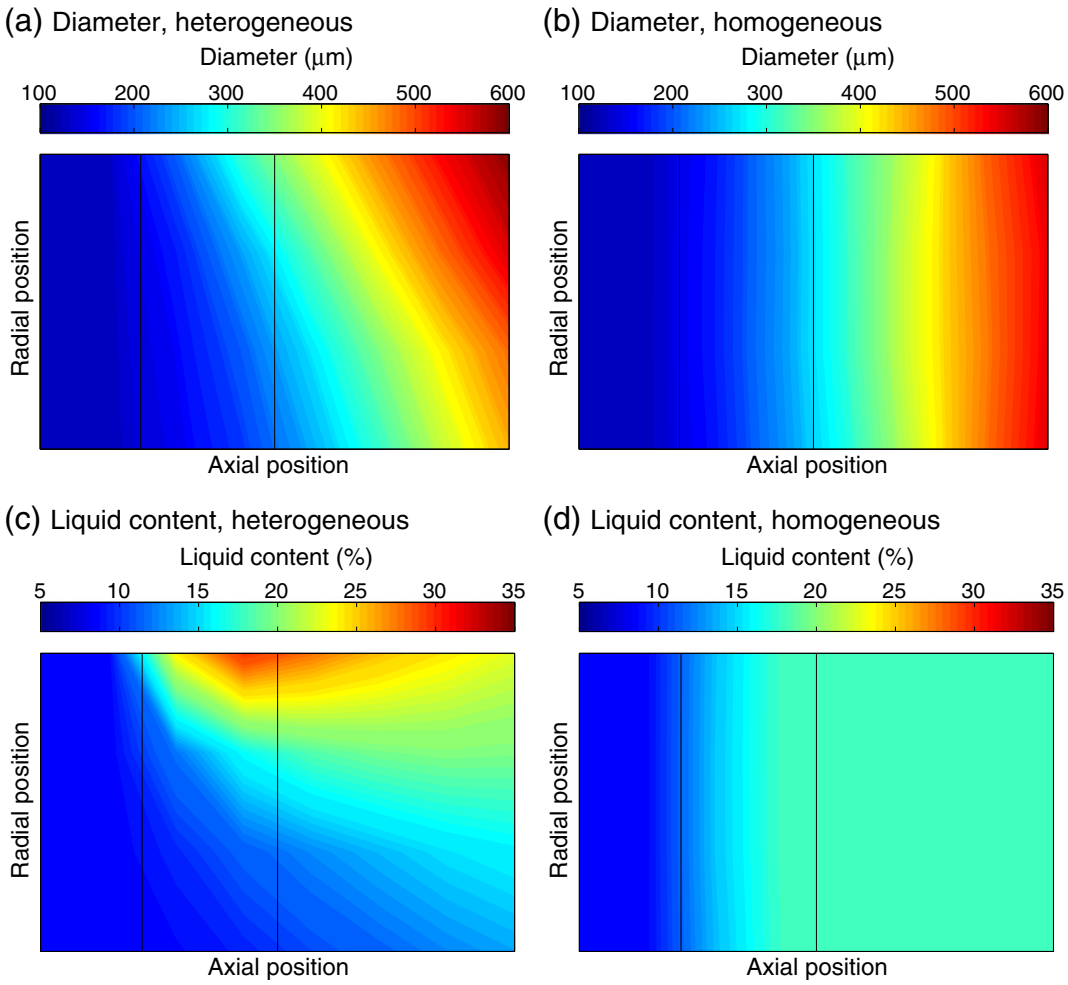

Fig. 7. Average diameter (a–b) and liquid content (c–d) versus position at steady state for the baseline case with heterogeneous and homogeneous liquid distributions. The vertical lines indicate the axial bounds of the spray zone.

3.2.2. Liquid to solids ratio

For both the homogeneous and heterogeneous cases, simulations were performed with varying liquid binder spray rates at three liquid-to-solid ratios (L/S): 0.05, 0.15 and 0.25. These ratios are typically used in experimental studies [17]. Fig. 8 shows the average diameter over time for each simulation. As expected, the simulations with a higher liquid spray rate produced larger granules. Because the aggregation rate is dependent on the liquid content, wetter particles aggregate more quickly. The steady-state average diameters at the highest L/S ratio were 562 μm and 597 μm, for the heterogeneous and homogeneous cases, respectively, compared with sizes of 472 μm and 482 μm for the lowest L/S ratio.

In all cases, the homogeneous liquid distribution produced a larger average diameter than the heterogeneous liquid distribution because in the heterogeneous case, some particles remained dry and were less likely to aggregate. This difference increased with increasing L/S ratio, which can be attributed to the bimodal liquid content distribution observed for the heterogeneous case, shown in Fig. 8. As the L/S ratio increased, the difference in liquid content between the wet and dry particles was greater, resulting in a larger difference between the two liquid distribution cases.

3.2.3. Spray zone

In addition to the spray rate, the length of the spray zone was also varied to simulate configurations with multiple sprayers, representing different process design options. Spray zone lengths of 4, 8, and 12 cm were simulated. The overall length of the granulator was held constant, as was the total spray rate. The length of the wet massing zone varied to accommodate these changes.

As seen in Fig. 9, a broader spray zone corresponded to smaller granules. The same total amount of liquid was added for each spray zone length. When the spray zone was small, the particles received the same amount of liquid more quickly, and when the spray zone was large, the liquid addition was spread across a larger region of particles. The sudden increase in liquid content that occurred in the 4-cm spray zone resulted in a rapid increase in diameter due to aggregation, while the size increase in the 12-cm spray zone was more gradual. Because the granulator with a 12-cm spray zone had a shorter wet massing zone, the granule size did not reach that of the 4-cm spray zone by the end of the granulator. In addition, the breakage rate was not substantial enough to mitigate the increase in diameter.

3.2.4. Granulator length

The effect of granulator length on the product was also observed to simulate another process design option. Three granulator lengths were simulated: 24, 32, and 40 cm. These changes were performed by varying the length of the wet massing zone, while keeping the lengths of the premixing and spray zones constant.

For these simulations, the residence time distribution (RTD) was evaluated. The RTD is important for blend homogeneity and compression characteristics. A longer residence time typically results in more consolidation and denser particles. Additionally, a narrower RTD could result in

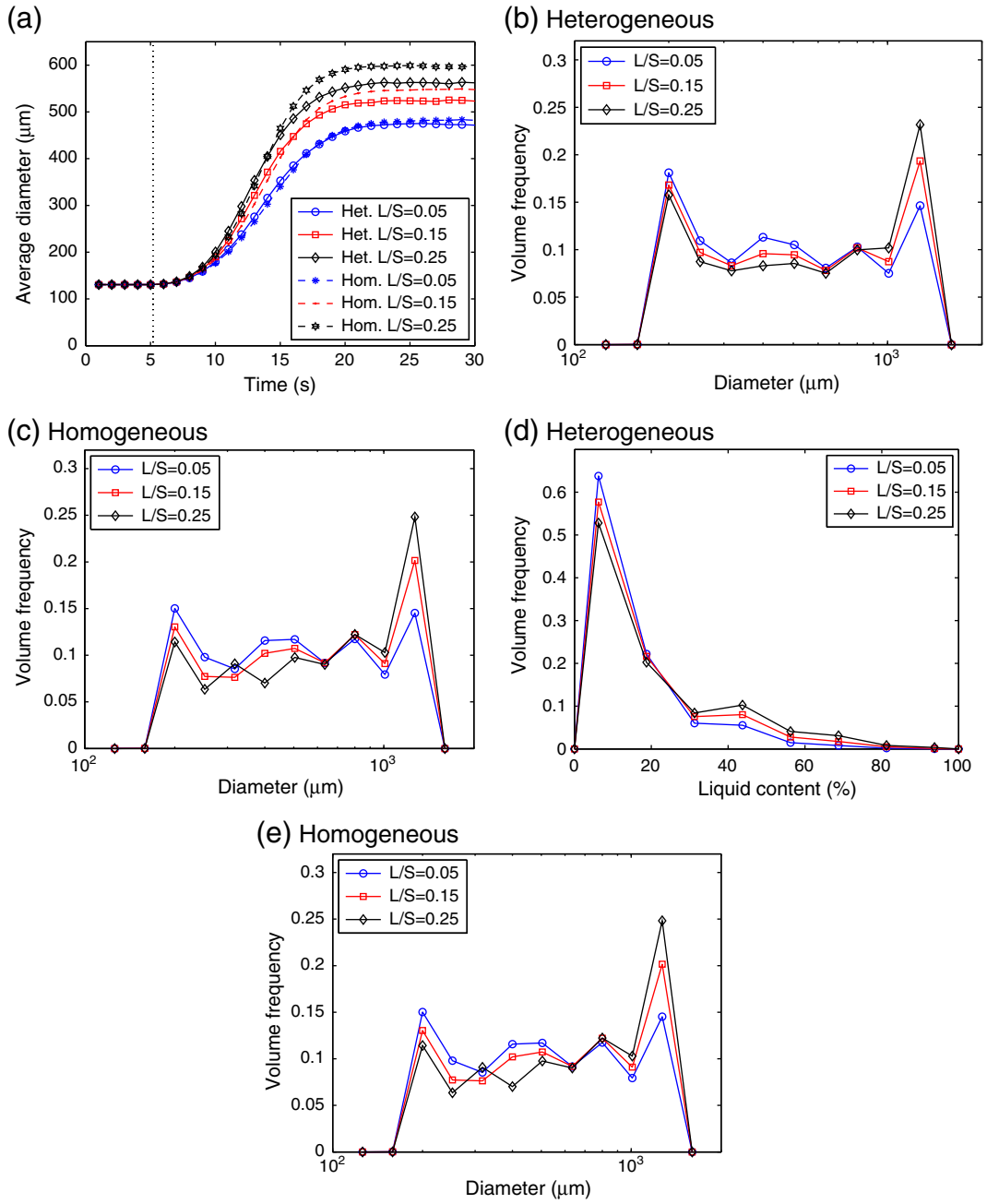

Fig. 8. (a) Average diameter at the outlet vs. time for varying L/S ratios, with a heterogeneous liquid distribution. The vertical dotted line indicates the time at which spraying begins. Steady-state (b–c), particle size and (d–e) liquid content distributions and for the baseline case with both liquid distribution models.

the granules being too porous hence resulting in tablets that are too hard because granules of low bulk density have a lower resistance to deformation during compression [46]. Therefore, RTD is an important characteristic to optimize. The residence time distribution was determined by simulating a pulse change in inlet composition after the process has reached a steady state. The initial inlet solid composition (x_0) was changed to a new composition (x_{pulse}) for one second by changing the fraction of feed particles in bin (1, 2, 1) from 0.25 to 1. The outlet composition (x_{out}) was recorded over time to calculate the exit age distribution, as shown in Eq. (25).

$$E(t) = \frac{x_{out} - x_0}{\int_0^\infty x_{out} - x_0 \, dt}. \tag{25}$$

The mean residence time ($\bar{t}$) was determined according to Eq. (26).

$$\bar{t} = \int_0^\infty tE(t)dt. \tag{26}$$

As shown in Fig. 10, a higher granulator length corresponded with a longer residence time. The mean residence times for granulators of lengths 24, 32, and 40 cm were 8.53 s, 11.2 s, and 13.9 s, respectively. Because of the greater residence time, longer granulators produced larger granules. Fig. 10 shows the particle size distributions at steady state with different granulator lengths, as well as the particle size distributions at the inlet and at the end of the spray zone. These distributions show some size enlargement in the spray zone, with bimodal distributions within the wet massing zone. While some larger particles form in

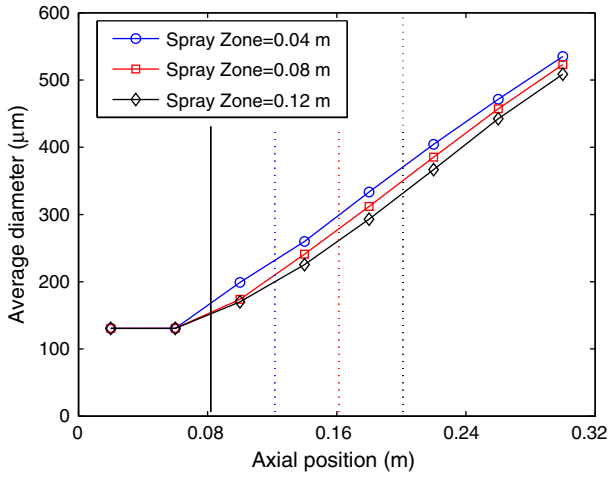

Fig. 9. Steady-state average diameter vs. position with varying spray zone lengths. The solid vertical line indicates the beginning of the spray zone, and the dotted vertical lines represent the ends of the spray zone for each length.

the spray zone, most of the agglomeration seems to occur within the wet massing zone.

Additionally, greater length corresponds to a larger average diameter. This relationship is shown in Fig. 10. While the case with heterogeneous liquid distribution shows a larger average diameter within the spray zone, the homogeneous case shows a larger average diameter at the outlet. This result can be attributed to a higher amount of dry, fine particles that do not participate in aggregation for the heterogeneous case. A plot of porosity versus position in Fig. 10 shows that the average porosity decreases in the premixing and wet massing zones, and increases in the spray zone. Because the porosity includes the liquid volume, an increase in liquid content results in an increased porosity. The average product porosity decreases with increased length because more consolidation occurs in the wet massing zone, due to the presence of residual liquid and minimal breakage and consolidation.

3.2.5. Particle velocities

The axial particle velocities were varied to simulate different screw speeds, an important process parameter. The baseline axial velocity was taken from the average residence time observed experimentally at a screw speed of 400 RPM [17]. By varying the radial velocity, different degrees of radial mixing are simulated. The particle velocity profiles are unknown, and a simple velocity model was assumed for this study. DEM simulations can be performed to better understand particle velocity profiles [47,48,39]. Future work will involve coupling DEM results with this model.

The values used for the axial velocity were 0.015, 0.03, and 0.045 m/s. The axial velocity was found to have a large effect on the product diameter, as shown in Fig. 11. A smaller axial velocity corresponded to a larger average particle size. This effect can be attributed to the larger residence time of slower-moving particles, also shown in Fig. 11. The evolution of granule size throughout the length of the granulator was affected by the velocity, also shown in Fig. 11. At higher velocities, the average diameter increases slightly in the spray zone, and more significantly in the wet massing zone. At lower velocities, the granule size increases

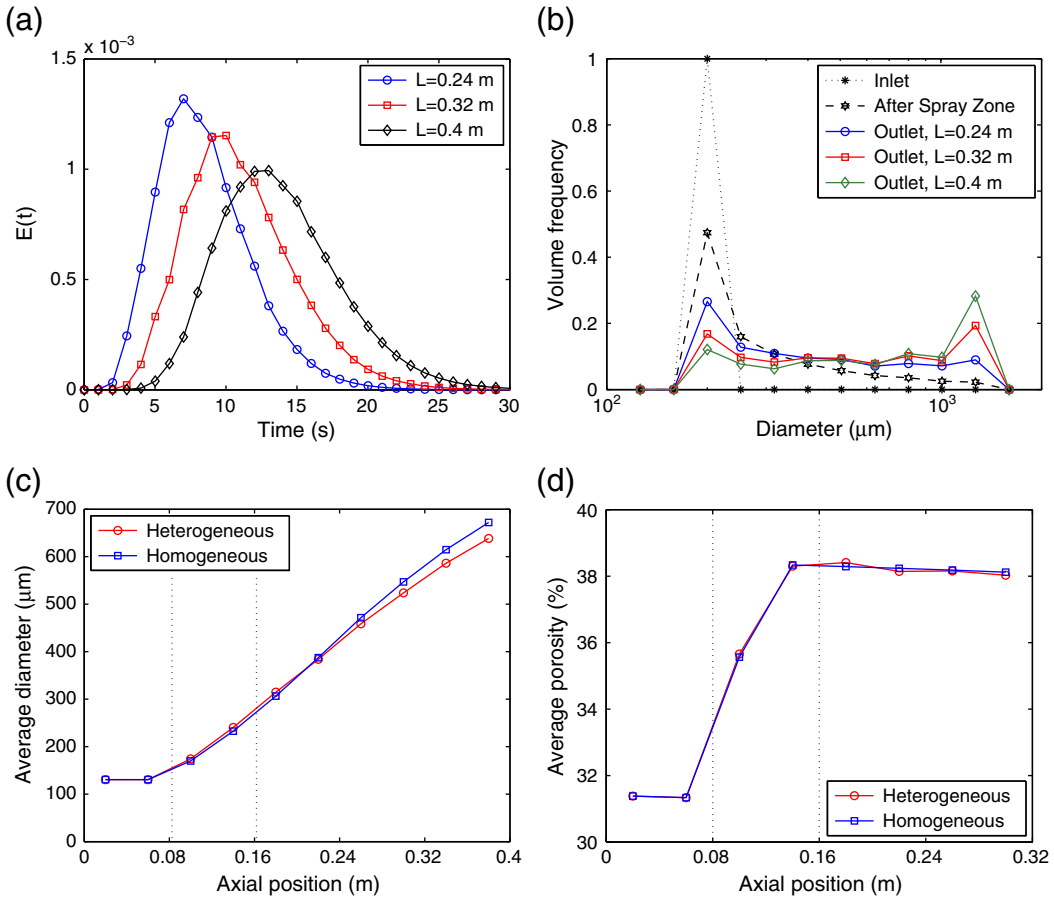

Fig. 10. (a) Residence time distributions for varying lengths. (b) Steady-state particle size distributions for varying lengths at the inlet, after the spray zone, and at the outlet. (c) Average diameter and (d) average porosity vs. axial position. The vertical lines indicate the axial bounds of the spray zone.

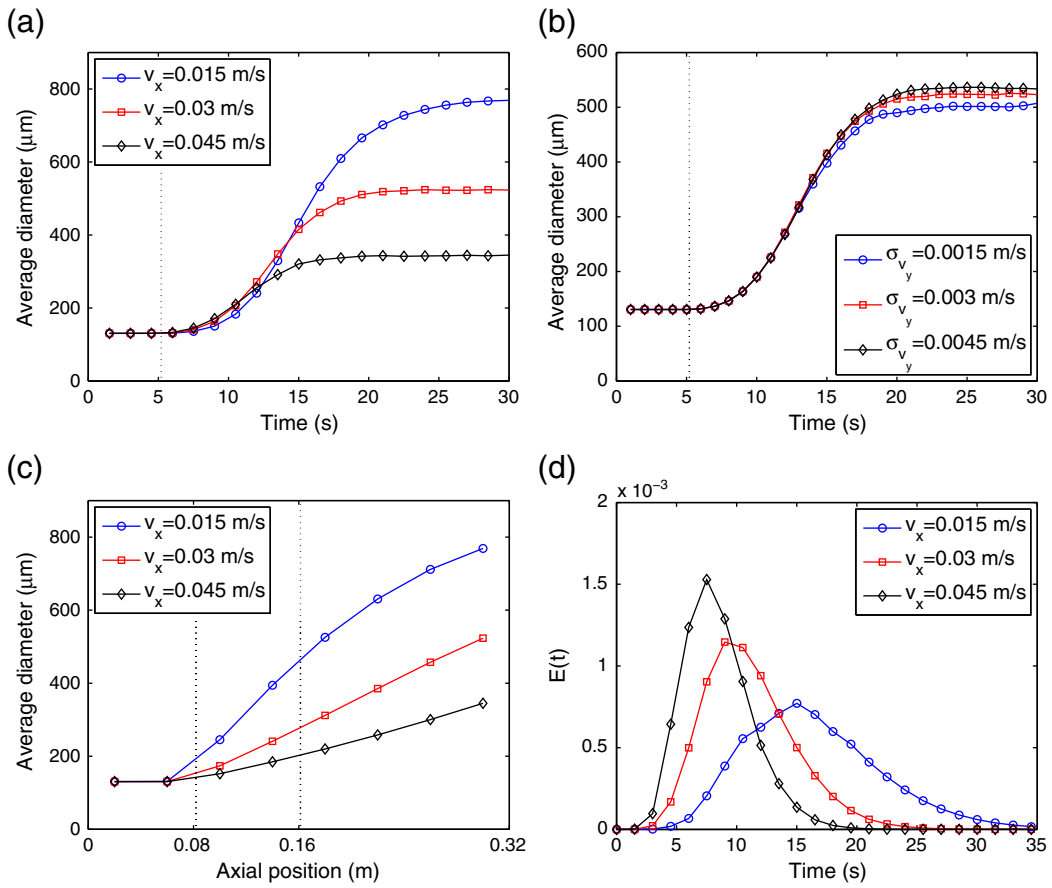

Fig. 11. Average diameter at the outlet vs. time for varying (a) axial and (b) radial velocities with heterogeneous liquid distribution, where vertical lines indicate the time at which spraying begins. (c) Average diameter vs. axial position for varying axial velocities, where vertical lines represent the axial bounds of the spray zone. (d) Residence time distributions for varying axial velocities.

more drastically in the spray zone, and at a lower rate in the wet massing zone, approaching a maximum value. Breakage rates are also reduced.

Since there was no net flux in the radial direction, the radial velocity was varied by changing the standard deviation of the randomly generated radial velocity. Values of 0.0015, 0.003, and 0.0045 m/s were selected. As shown in Fig. 11, the heterogeneous simulations with a smaller radial velocity resulted in smaller granules. When the radial velocity is high, there is a large amount of mixing between bins along the radial axis, spreading the liquid binder throughout the granulator more evenly.

3.2.6. API–excipient interaction

To represent multi-component granulation, interactions between the API and excipient particles were taken into account. Repulsion between the API and excipient can cause segregation and inhomogeneous granule composition, which can affect the final product. By varying the parameter a_{ab} in the aggregation kernel with values of −2 and 2, attractive and repulsive interactions were simulated. In the baseline case, no interaction was assumed, and this parameter was equal to zero. The aggregation coefficient β_0 was adjusted to yield the same aggregation rate for the initial powder particles with particles of the same type across the three cases. In practice, the interaction parameter would be evaluated experimentally for the specific API and excipient in question.

As expected, Fig. 12 shows that the average diameter is smaller when the components are repulsive and larger when they are attractive. The aggregation rates between dissimilar particles are greater for attractive interactions than for repulsive interactions. As a result, attractive interactions between the API and excipient result in larger particles with more uniform compositions. Further, distributions in composition, presented in Fig. 12 show that the case involving attraction produces more granules with even compositions, while the repulsive case has a slightly larger fraction of purer particles, at the extreme ends of composition. In the case with no interaction, two peaks are still present, indicating that some of the API and excipient particles remain segregated as particles, though they are spatially mixed. Due to the short residence time in the granulator, some of the primary particles did not aggregate significantly, and remained in the product stream as fine API or excipient particles.

3.3. Comparison with experimental trends

The simulated bulk and distributed profiles are consistent with experimental results for twin screw granulation. Similar to the model results, Keleb et al. [16] and El Hagrasy et al. [17] observed bimodal particle size distributions. Further, Keleb et al. [16] found that an increase in screw speed resulted in a decrease in granule yield. The model demonstrates that an increase in axial velocity decreases the residence time, resulting in a larger fraction of unaggregated fines.

Dhenge et al. [49] and El Hagrasy et al. [17] demonstrated a correlation between the L/S ratio and granule size. Larger granules form at higher L/S ratios, consistent with the liquid-dependent aggregation kernel implemented in the model. Fig. 13 shows the size distributions observed experimentally by El Hagrasy et al. [17] at different L/S ratios. They found a reduced fraction of powder fines at high L/S ratios, as well as a wider size distribution. While our simulated results show a wide size distribution at high L/S ratios, the fraction of fines decreases, and the peak within the granule size range becomes more prominent, as shown in Fig. 8.

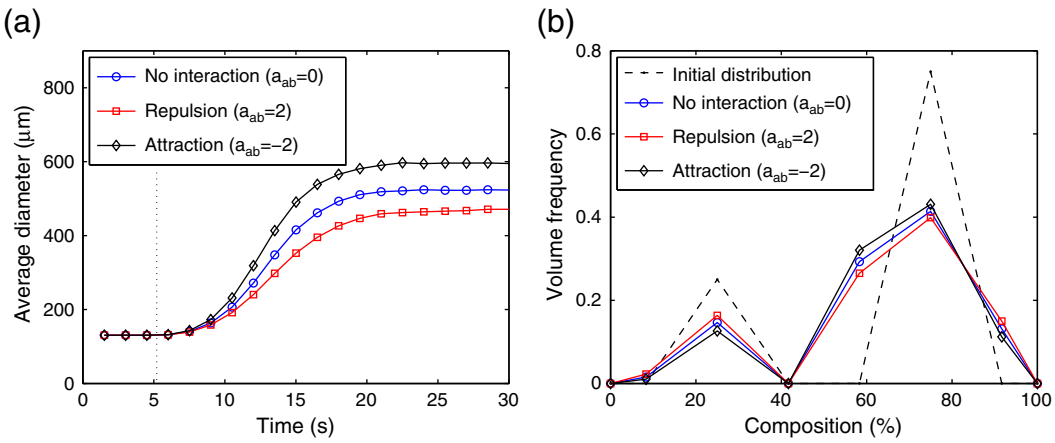

Fig. 12. (a) Average diameter over time with varying API–excipient interactions and (b) steady-state compositional distributions. The vertical dotted line indicates the time at which spraying begins.

El Hagrasy et al. [17] found that some very large granules were produced, even at low L/S ratios. They attribute this observation to the kneading blocks of the screws, which were unable to adequately distribute the liquid binder. Similarly, in the simulations, poor liquid distribution resulted in wide size distributions, with some very large particles and a high fraction of fines.

In order to establish a more quantitatively accurate model, a more detailed understanding of the flow behavior of the granules must be developed. It was observed that the particle velocities and distribution of the liquid binder have large affects on the granule size distributions. Additionally, semi-empirical rate kernels were implemented, which contain some adjustable parameters. These parameters can be estimated using experimental data to develop a more robust model.

The model provides additional insight into the experimental results, demonstrating variations in time and space. The particle size distribution can be predicted at each position, illustrating the effects of each zone. Multi-dimensional distributions can be modeled, enabling inhomogeneities in size, composition, and liquid distribution to be simulated.

4. Conclusions

Continuous granulation processes have potential advantages over batch processes in pharmaceutical manufacturing. Continuous granulation can be simulated using PBMs with spatial coordinates. These models are useful in process development, validation, and control.

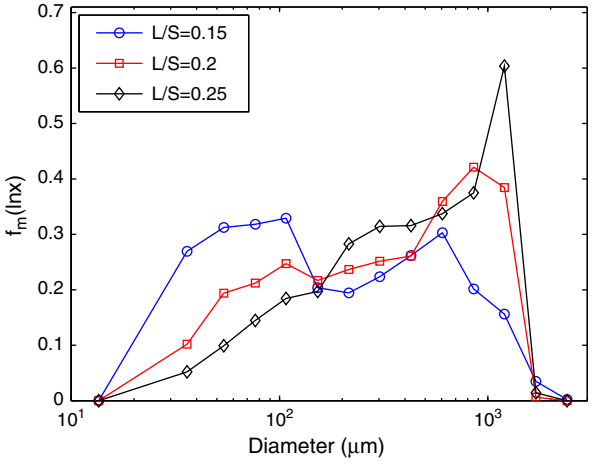

Fig. 13. Experimentally observed granule size distributions using pharmatose 200 M lactose in a twin screw granulator with varying L/S ratios [17].

For the first time, a developed model was able to simulate particle distributions in size, composition, liquid binder content, and evolution of porosity, taking into account the rate processes of aggregation, liquid addition, consolidation, and breakage. It also considers the interactions between multiple solid components and the incorporation of particle flux information.

The results show good agreement with experimental trends, such as the bimodal size distributions, the relationship between granule size and liquid spray rate, and the effects of poor liquid distribution. For more quantitatively accurate predictions, a better understanding of the flow properties within the granulator is needed.

Additionally, future work will investigate the rate kernels and their adjustable constants. Parameter estimation using experimental data can be used to evaluate adjustable constants in the rate kernels. A variety of empirical rate kernels are used in the literature [2], and mechanistic kernels have also been developed [23,50]. With substantial experimental data, these kernels can be compared and evaluated within the framework of this model.

There are various practical uses for a validated, accurate model of continuous granulation processes, particularly in pharmaceutical process design. As a part of the ERC-SOPs, a pilot plant for continuous tablet manufacturing is being assembled at Rutgers University. This approach has potential advantages over traditional batch methods in process control, efficiency, and cost. As continuous processing is investigated as an alternative to batch processes, the developed process model is useful in design and optimization, particularly to define a design space and implement QbD. In addition, these models can be used to develop model-based process control and optimization strategies.

Acknowledgments

This work is supported by the National Science Foundation Engineering Research Center on Structured Organic Particulate Systems Grant NSF-ECC 0540855. The authors would also like to acknowledge ERC-SOPS colleagues Prof. James D. Litster and Dr. Arwa El Hagrasy in Purdue University for providing experimental data. S. Walia would like to acknowledge the Research in Science and Engineering (RISE) program at Rutgers/UMDNJ for funding.

References

[1] Simon M. Iveson, James D. Litster, Karen Hapgood, Bryan J. Ennis, Nucleation, growth and breakage phenomena in agitated wet granulation processes: a review, Powder Technology 117 (12) (2001) 3–39.
[2] I.T. Cameron, F.Y. Wang, C.D. Immanuel, F. Stepanek, Process systems modelling and applications in granulation: a review, Chemical Engineering Science 60 (14) (2005) 3723–3750.

[3] Fu Yang Wang, Ian T. Cameron, Review and future directions in the modelling and control of continuous drum granulation, Powder Technology 124 (3) (2002) 238–253.
[4] Chris Vervaet, Jean Paul Remon, Continuous granulation in the pharmaceutical industry, Chemical Engineering Science 60 (14) (2005) 3949–3957.
[5] Hans Leuenberger, New trends in the production of pharmaceutical granules: batch versus continuous processing, European Journal of Pharmaceutics and Biopharmaceutics 52 (3) (2001) 289–296.
[6] Hans Leuenberger, Scale-up in the 4th dimension in the field of granulation and drying or how to avoid classical scale-up, Powder Technology 130 (13) (2003) 225–230.
[7] K. Plumb, Continuous processing in the pharmaceutical industry: changing the mind set, Chemical Engineering Research and Design 83 (6) (2005) 730–738.
[8] Spencer D. Schaber, Dimitrios I. Gerogiorgis, Rohit Ramachandran, James M.B. Evans, Paul I. Barton, Bernhardt L. Trout, Economic analysis of integrated continuous and batch pharmaceutical manufacturing: a case study, Industrial and Engineering Chemistry Research 50 (17) (2011) 10083–10092.
[9] A. Faure, P. York, R.C. Rowe, Process control and scale-up of pharmaceutical wet granulation processes: a review, European Journal of Pharmaceutics and Biopharmaceutics 52 (3) (2001) 269–277.
[10] Thomas Glaser, Constantijn F.W. Sanders, Fu.Y. Wang, Ian T. Cameron, James D. Litster, Jonathan M.-H. Poon, Rohit Ramachandran, Charles D. Immanuel, Francis J. Doyle III, Model predictive control of continuous drum granulation, Journal of Process Control 19 (4) (2009) 615–622.
[11] Rohit Ramachandran, Anwesha Chaudhury, Model-based design and control of a continuous drum granulation process, Chemical Engineering Research and Design 90 (8) (2012) 1063–1073.
[12] Rohit Ramachandran, Jeyrathan Arjunan, Anwesha Chaudhury, Marianthi Ierapetritou, Model-based control-loop performance of a continuous direct compaction process, Journal of Pharmaceutical Innovation 6 (2011) 249–263.
[13] Fani Boukouvala, Atul Dubey, Aditya Vanarase, Rohit Ramachandran, Fernando J. Muzzio, Marianthi Ierapetritou, Computational approaches for studying the granular dynamics of continuous blending processes, 2 — population balance and data-based methods, Macromolecular Materials and Engineering 297 (1) (2012) 9–19.
[14] Fani Boukouvala, Rohit Ramachandran, Aditya Vanarase, Fernando J. Muzzio, Marianthi G. Ierapetritou, Computer aided design and analysis of continuous pharmaceutical manufacturing processes, in: M.C. Georgiadis, E.N. Pistikopoulos, A.C. Kokossis (Eds.), 21st European Symposium on Computer Aided Process Engineering, Computer Aided Chemical Engineering, volume 29, Elsevier, 2011, pp. 216–220.
[15] Fani Boukouvala, Vasilios Niotis, Rohit Ramachandran, Fernando J. Muzzio, Marianthi G. Ierapetritou, An integrated approach for dynamic flowsheet modeling and sensitivity analysis of a continuous tablet manufacturing process, Computers and Chemical Engineering 42 (2012) 30–47.
[16] E.I. Keleb, A. Vermeire, C. Vervaet, J.P. Remon, Twin screw granulation as a simple and efficient tool for continuous wet granulation, International Journal of Pharmaceutics 273 (12) (2004) 183–194.
[17] A.S. El Hagrasy, J.R. Hennenkamp, M.D. Burke, J.J. Cartwright, J.D. Litster, Twin screw wet granulation: influence of formulation parameters on granule properties and growth behavior, Powder Technology 238 (2013) 108–115.
[18] Gavin M. Walker, Chapter 4 — drum granulation processes, in: M.J. Hounslow, A.D. Salman, J.P.K. Seville (Eds.), Granulation, Handbook of Powder Technology, volume 11, Elsevier Science B.V., 2007, pp. 219–254.
[19] Doraiswami Ramkrishna, Chapter 4 — the solution of population balance, Population Balances, Academic Press, San Diego, 2000, pp. 117–195.
[20] Charles David Immanuel, Francis Joseph Doyle III, Solution technique for a multi-dimensional population balance model describing granulation processes, Powder Technology 156 (23) (2005) 213–225.
[21] Jonathan M.-H. Poon, Rohit Ramachandran, Constantijn F.W. Sanders, Thomas Glaser, Charles D. Immanuel, Francis J. Doyle III, James D. Litster, Frantisek Stepanek, Fu-Yang Wang, Ian T. Cameron, Experimental validation studies on a multi-dimensional and multi-scale population balance model of batch granulation, Chemical Engineering Science 64 (4) (2009) 775–786.
[22] Rohit Ramachandran, Jonathan M.-H. Poon, Constantijn F.W. Sanders, Thomas Glaser, Charles D. Immanuel, Francis J. Doyle III, James D. Litster, Frantisek Stepanek, Fu-Yang Wang, Ian T. Cameron, Experimental studies on distributions of granule size, binder content and porosity in batch drum granulation: inferences on process modelling requirements and process sensitivities, Powder Technology 188 (2) (2008) 89–101.
[23] Jonathan M.-H. Poon, Charles D. Immanuel, Francis J. Doyle III, James D. Litster, A three-dimensional population balance model of granulation with a mechanistic representation of the nucleation and aggregation phenomena, Chemical Engineering Science 63 (5) (2008) 1315–1329.
[24] Rohit Ramachandran, Paul I. Barton, Effective parameter estimation within a multi-dimensional population balance model framework, Chemical Engineering Science 65 (16) (2010) 4884–4893.
[25] Rohit Ramachandran, Mansoor A. Ansari, Anwesha Chaudhury, Avi Kapadia, Anuj V. Prakash, Frantisek Stepanek, A quantitative assessment of the influence of primary particle size polydispersity on granule inhomogeneity, Chemical Engineering Science 71 (2012) 104–110.
[26] Dana Barrasso, Rohit Ramachandran, A comparison of model order reduction techniques for a four-dimensional population balance model describing multi-component wet granulation processes, Chemical Engineering Science 80 (2012) 380–392.
[27] Simon M. Iveson, Limitations of one-dimensional population balance models of wet granulation processes, Powder Technology 124 (3) (2002) 219–229.
[28] C.A. Biggs, C. Sanders, A.C. Scott, A.W. Willemse, A.C. Hoffman, T. Instone, A.D. Salman, M.J. Hounslow, Coupling granule properties and granulation rates in high-shear granulation, Powder Technology 130 (13) (2003) 162–168.
[29] Daan Verkoeijen, Gerard A. Pouw, Gabriel M.H. Meesters, Brian Scarlett, Population balances for particulate processes—a volume approach, Chemical Engineering Science 57 (12) (2002) 2287–2303.
[30] Anwesha Chaudhury, Alexander Niziolek, Rohit Ramachandran, Multi-dimensional mechanistic modeling of fluid bed granulation processes: an integrated approach, Advanced Powder Technology 24 (1) (2013) 113–131.
[31] T. Matsoukas, C.L. Marshall Jr., Bicomponent aggregation in finite systems, Europhysics Letters 92 (4) (2010) 46007.
[32] Carl L. Marshall Jr., Pavol Rajniak, Themis Matsoukas, Multi-component population balance modeling of granulation with continuous addition of binder, Powder Technology 236 (2013) 211–220.
[33] K. Lee, T. Kim, P. Rajniak, T. Matsoukas, Compositional distributions in multicomponent aggregation, Chemical Engineering Science 63 (5) (2008) 1293–1303.
[34] Stefan Heinrich, Mirko Peglow, Lothar Morl, Unsteady and steady-state particle size distributions in batch and continuous fluidized bed granulation systems, Chemical Engineering Journal 86 (12) (2002) 223–231.
[35] Stefan Heinrich, Mirko Peglow, Matthias Ihlow, Markus Henneberg, Lothar Morl, Analysis of the start-up process in continuous fluidized bed spray granulation by population balance modelling, Chemical Engineering Science 57 (20) (2002) 4369–4390.
[36] A. Gerstlauer, S. Motz, A. Mitrovic, E.-D. Gilles, Development, analysis and validation of population models for continuous and batch crystallizers, Chemical Engineering Science 57 (20) (2002) 4311–4327.
[37] Maitraye Sen, Rohit Ramachandran, A multi-dimensional population balance model approach to continuous powder mixing processes, Advanced Powder Technology 24 (1) (2013) 51–59.
[38] Carl L. Marshall Jr., Pavol Rajniak, Themis Matsoukas, Numerical simulations of two-component granulation: comparison of three methods, Chemical Engineering Research and Design 89 (5) (2011) 545–552.
[39] Patricia M. Portillo, Fernando J. Muzzio, Marianthi G. Ierapetritou, Hybrid DEM-compartment modeling approach for granular mixing, AIChE Journal 53 (1) (2007) 119–128.
[40] Ranjit M. Dhenge, Kimiaki Washino, James J. Cartwright, Michael J. Hounslow, Agba D. Salman, Twin screw granulation using conveying screws: effects of viscosity of granulation liquids and flow of powders, Powder Technology 238 (2013) 77–90.
[41] L. Madec, L. Falk, E. Plasari, Modelling of the agglomeration in suspension process with multidimensional kernels, Powder Technology 130 (13) (2003) 147–153.
[42] T. Matsoukas, T. Kim, K. Lee, Bicomponent aggregation with composition-dependent rates and the approach to well-mixed state, Chemical Engineering Science 64 (4) (2009) 787–799.
[43] J.D. Pandya, L.A. Spielman, Floc breakage in agitated suspensions: effect of agitation rate, Chemical Engineering Science 38 (12) (1983) 1983–1992.
[44] J. Kumar, M. Peglow, G. Warnecke, S. Heinrich, L. Morl, Improved accuracy and convergence of discretized population balance for aggregation: the cell average technique, Chemical Engineering Science 61 (10) (2006) 3327–3342.
[45] Anwesha Chaudhury, Avi Kapadia, Anuj V. Prakash, Dana Barrasso, Rohit Ramachandran, An extended cell-average technique for multi-dimensional population balance models describing aggregation and breakage, Advanced Powder Technology (in press) http://dx.doi.org/10.1016/j.apt.2013.01.006.
[46] J. Vercruysse, D. Cordoba Diaz, E. Peeters, M. Fonteyne, U. Delaet, I. Van Assche, T. De Beer, J.P. Remon, C. Vervaet, Continuous twin screw granulation: influence of process variables on granule and tablet quality, European Journal of Pharmaceutics and Biopharmaceutics 82 (1) (2012) 205–211.
[47] Justin A. Gantt, Edward P. Gatzke, High-shear granulation modeling using a discrete element simulation approach, Powder Technology 156 (23) (2005) 195–212.
[48] Justin A. Gantt, Ian T. Cameron, James D. Litster, Edward P. Gatzke, Determination of coalescence kernels for high-shear granulation using DEM simulations, Powder Technology 170 (2) (2006) 53–63.
[49] Ranjit M. Dhenge, Richard S. Fyles, James J. Cartwright, David G. Doughty, Michael J. Hounslow, Agba D. Salman, Twin screw wet granulation: granule properties, Chemical Engineering Journal 164 (23) (2010) 322–329.
[50] Rohit Ramachandran, Charles D. Immanuel, Frantisek Stepanek, James D. Litster, Francis J. Doyle III, A mechanistic model for breakage in population balances of granulation: theoretical kernel development and experimental validation, Chemical Engineering Research and Design 87 (4) (2009) 598–614.